Effects of age on resting-state cortical networks

Chetan Gohil[1], Oliver Kohl[1], Jemma Pitt[1], Mats W.J. van Es[1], Andrew J. Quinn[2], Diego Vidaurre[3], Martin R. Turner[4], Anna C. Nobre[5,6], and Mark W. Woolrich[1]

[1]Oxford Centre for Human Brain Activity, Wellcome Centre for Integrative Neuroimaging, Department of Psychiatry, University of Oxford, Oxford, UK
[2]Centre for Human Brain Health, School of Psychology, University of Birmingham, Birmingham, UK
[3]Center of Functionally Integrative Neuroscience, Department of Clinical Medicine, Aarhus University, Aarhus, Denmark
[4]Nuffield Department of Clinical Neurosciences, University of Oxford, Oxford, UK
[5]Wu Tsai Institute, Yale University, New Haven, CT, USA
[6]Department of Psychology, Yale University, New Haven, CT, USA

September 20, 2024

Abstract

Magnetoencephalography recordings of functional brain activity reveal large-scale cortical networks that are associated with cognition. The correlation of individualised networks with age and cognitive performance (*age effects* and *cognitive performance effects* respectively) was studied using a large cross-sectional healthy cohort ($N = 612$, 18-88 years old) and accounting for a comprehensive set of confounds. Age effects were found in time-averaged functional networks in five canonical frequency bands (δ, θ, α, β, γ) that are consistent with the posterior-anterior shift with age observed in functional magnetic resonance imaging. Evidence from cognitive performance effects in time-averaged networks suggested the importance of maintaining α-band activity for cognitive health. A more detailed description of the functional activity was obtained by adopting an established machine learning approach (the Hidden Markov Model). Ten transient large-scale cortical networks with fast dynamics ($\sim$100 ms) were identified, which provided insight into age and cognitive performance effects that were not observed in the time-averaged analyses. The time spent in most networks increased with age, whereas the time spent in frontal networks decreased. The cognitive performance effects for the transient networks suggested that age effects in the frontal networks are compensatory. Thus, our study suggests both the maintenance of functional activity (lesser age effects) and the recruitment of compensatory functional activity can co-occur to produce good cognitive performance in older individuals. The time-averaged and transient functional networks have been made publicly available as a resource.

1 Introduction

With an increasing proportion of elderly people globally [1], there is a pressing need to understand age-related changes in functional brain activity. It is important to separate changes associated with healthy cognition from those that lead to cognitive decline, or are linked to specific age-associated diseases. This could facilitate the early detection of pathology and development of preventative intervention [2].

An observed property of the functional activity from neuronal populations and circuits is the emergence of *neuronal oscillations* [3]. It is widely believed that cognition is facilitated by large-scale functional networks [4, 5], in which neuronal oscillations help regulate the routing of information [6, 7]. Note that functional network activity is transient in nature [9]. Magnetoencephalography (MEG) [8] can be used non-invasively to estimate these large-scale functional brain networks of oscillatory activity at millisecond timescales [9, 10]. Note, this is a perspective that cannot be obtained using functional magnetic resonance imaging (fMRI) due to it being a slower indirect measure of neuronal activity [11].

Although there have been several studies looking at the relationship between neuronal oscillations and age for healthy individuals using electroencephalography (EEG) data, MEG studies are limited and the large-scale network perspective is yet to be fully explored [13, 14, 24]. In this study, we looked at the correlates of age and cognitive performance (*age effects* and *cognitive performance effects* respectively, see Section 2.4) in large-scale functional brain networks using resting-state MEG recordings from a large cohort of healthy individuals (612 subjects, 18-88 years old). Both time-averaged (static) and transient (dynamic) networks are studied. To the authors' knowledge, this is the first study to look at age and cognitive performance effects in transient large-scale functional networks of oscillatory activity.

2 Materials and Methods

2.1 Dataset

In the current work, we study a cross-sectional group of 612[1] healthy subjects aged between 18 and 88 years from the Cam-CAN (Cambridge Centre for Ageing and Neuroscience) dataset. The demographics of these subjects are shown in Figure S1. Each subject has a resting-state[2] (eyes closed) MEG recording, structural MRI (sMRI) and a set of cognitive task scores. Further information regarding the dataset and protocols is provided in [27, 28].

MEG data. The MEG recordings were obtained using a 306 channel Vectorview system (Elekta Neuromag, Helsinki, Finland), consisting of 102 magnetometers and 204 orthogonal planar gradiometers. The acquisition time of the recordings was 8 minutes 40 seconds, with the first 20 seconds discarded. The data were recorded at a sampling frequency of 1 kHz and bandpass filtered between 0.03 Hz and 330 Hz.

sMRI data. T1-weighted sMRIs were acquired using a 4 minutes 32 seconds MPRAGE (Magnetization-Prepared RApid Gradient Echos) sequence with a 3 T TIM Trio scanner (Siemens Healthcare, Erlangen, Germany) equipped with a 32-channel head coil.

Cognitive task scores. Five board cognitive domains were evaluated using a set of tasks (executive function, language, emotion, memory, motor control). We drew from the same 13 cognitive task scores as [25], provided by [30]. We study the 10 cognitive tasks summarised in Table 1. Three cognitive tasks (Face Recognition, Spot the Word, Proverb Comprehension) were excluded due to their incompatibility with PCA for dimensionality reduction (their distribution was highly non-Gaussian or discrete). See [30] for a complete description of the tasks.

To reduce the cognitive task scores into a single metric for performance, we concatenated the scores into a vector for each subject and applied PCA across subjects. Taking the first principal component gives a single number that quantifies the performance of a subject in all of the cognitive tasks. Figure 3A shows the PCA loadings (with the contribution of each cognitive task to the principal component). All PCA loadings have positive values, indicating an increase in the first principal component results in an increase in all cognitive task scores.

Table 1: Tasks used for evaluating cognitive performance. See [30] for a detailed description of each task.

Domain	**Task**
Executive Function	Fluid Intelligence (FldIn)
	Multitasking (MltTs)
Language Functions	Sentence Comprehension (SntRec)
	Picture-Picture Priming (PicName)
	Verbal Fluency (VrbFl)
Emotional Processing	Emotion Expression Recognition (EmoRec)
Memory	Visual Short-Term Memory (VSTM)
	Story Recall (StrRec)
Processing Speed	Choice Motor Speed (MRSp)
	Choice Motor Coefficient of Variation (MRCv)

[1]The Cam-CAN dataset contained 643 subjects with MEG recordings, of which 22 did not have sMRIs and 9 failed in the sMRI surface extraction.

[2]Also known as *spontaneous* or *task free* activity.

2.1.1 MEG Preprocessing, Source Reconstruction and Parcellation

The Cam-CAN MEG data were processed using the OHBA Software Library (OSL) [31]. For each subject, we applied the following steps:

1. **MaxFilter**. The raw MEG recordings were first MaxFiltered (using v2.2.12). This is an algorithm used to remove noise originating from outside the scanner from the MEG recordings. Temporal signal source space separation (tSSS) [32] was applied (correlation threshold 0.98, 10 s sliding window) with head-motion correction (using 200 ms windows). We used the MaxFiltered MEG data (with movement compensation, without default transformation) provided by Cam-CAN.

2. **Filtering and downsampling**. First, we bandpass filtered the data (fifth-order IIR Butterworth) between 1 and 125 Hz, then applied notch filters (2 Hz width) at 50 Hz and 100 Hz to remove mains artefacts and an additional spike artefact at 88 Hz. Following this, the data were downsampled to 250 Hz.

3. **Automated bad segment/channel detection**. Bad segments and channels can have a detrimental effect on independent component analysis (ICA) denoising (next step). Therefore, we annotated significantly high variance (p-value < 0.1) using an automated generalised-extreme studentised deviate (G-ESD) algorithm [33]. Bad segment and channel detection was applied separately to the different sensor types (magnetometers and gradiometers).

4. **ICA artefact removal**. After excluding the bad segments and channels, we applied FastICA [34] to the sensor-level MEG data, decomposing the signal into 64 independent components. Based on the correlation of the source time courses with the EOG/ECG electrodes (0.9 threshold), independent components were marked as ocular/cardiac noise and removed from the MEG data.

5. **Bad channel interpolation**. Bad channels in the ICA-cleaned MEG data were replaced using a spherical spline interpolation [35]. This was the final step in preprocessing the sensor-level MEG data.

6. **Coregistration**. Scalp, inner skull, and outer brain surface were extracted from the sMRI using FSL BET [36, 37]. The nose was not included in the scalp surface because the sMRI images were defaced. The scalp surface was then used in OSL RHINO [31] to coregister the sMRI to the MEG data based on matching the scalp to a set of digitised Polhemus head shape points and fiducials, whose positions relative to the sensors were known via the head-position coils.

7. **Forward modelling**. The *forward model* gives us the expected signal at each sensor (leadfield) for a dipole placed at a particular location inside the brain. The magnetic field from this dipole transverses different tissue types, which have different electromagnetic properties. It is common in MEG source localisation to model the changes in electromagnetic properties using a single boundary separating the volume inside the brain from outside. In the current work, we used a boundary element model [38], using the inner skull surface as the boundary. We calculated the leadfields for a dipole placed in the x, y and z-direction on an 8 mm isotropic grid inside the volume bound by the inner skull.

8. **Bandpass filtering and bad segment removal**. We applied a bandpass filter to the preprocessed MEG data (firth-order IIR Butterworth) to focus on the frequency range of interest, which is 1-80 Hz, and removed bad segments from the data to ensure these did not impact on the quality of the source localisation (next step).

9. **Volumetric beamforming**. We employed a beamformer [39, 10] to source localise the MEG data. The beamformer estimates source activity (at a location inside the brain) as a linear combination of sensor activity. In this step, we calculated the weights for the linear combination, referred to as the *beamformer weights*. We used a unit-noise-gain invariant Linearly Constrained Minimum Variance (LCMV) beamformer. This type of beamformer controls for the depth bias by normalising the beamformer weights [40].

   To calculate the beamformer weights, we need provide the leadfields from the forward model, the covariance of noise (signal measured by the sensors unrelated to brain activity) and the covariance of the data (signal measured by the sensors containing both noise and brain activity). For the noise covariance, we used a diagonal matrix containing the variance of each sensor type. We filled the diagonal elements corresponding to magnetometers (gradiometers) with the average (temporal) variance across all magnetometers (gradiometers). For the data covariance, we used the covariance of the data from step 8 reduced to a rank of 60 (this regularisation improves the robustness of the beamformer).

   The beamformer calculates the activity in the x, y and z-direction at each grid point used in the leadfield calculation. This is reduced to a single value by projecting the x, y, z activity onto the axis that maximises power of at that location. The sensor activity at each time point is beamformed independently. After beamforming, we are left with the activity at each grid point inside the brain, referred to as a *voxel*.

10. **Parcellation**. Often, we have a very large number of voxels, so we parcellate the data into particular regions of interest (ROIs). In the current work, we used an anatomically defined 52-ROI parcellation. See [41] for a description of the parcellation. Parcel time courses were obtained by applying PCA to the (demeaned) voxel time courses assigned to a parcel and taking the first principal component. PCA is preferred over simply taking the mean across voxels because there is a sign ambiguity in the voxel time courses due to the beamformer.

11. **Orthogonalisation**. The source localisation of MEG data suffers from spatial leakage where the uncertainty in estimating source activity leads to nearby locations in source space exhibiting highly correlated activity. These correlations can be misinterpreted as functional connectivity (so called 'ghost interactions' [42]). To minimise the impact of spatial leakage, we used the symmetric orthogonalisation technique proposed in [42], which removes all zero-lag correlations from the parcel data. This can be seen as a conservative approach as we have likely removed some genuine zero-lag functional connectivity from the data.

12. **Sign flipping**. Unfortunately, there is an ambiguity in the sign of each parcel time course (due to the PCA and beamformer). This means the sign of each parcel time course can be misaligned across subjects. After we have the parcel time courses for each subject, we selected the median subject as a template (based on the average correlation between covariance matrices for a subject compared to all other subjects). Then we matched the sign of each subject's orthogonalised parcel time course to the template using the random search sign-flip algorithm described in [9].

Note, in the current work all references to the 'parcel time courses' are to the sign-flipped orthogonalised parcel time courses.

2.2 Time-Averaged Network Analysis

We assessed the impact of healthy biological ageing on the following time-averaged properties of source-localised MEG data: power spectral density (PSD), power, coherence, and α-peak

frequency. The calculation of these quantities is described below. Figure S4 summarises the steps.

Power/coherence spectra. We used Welch's method [43] (2 s Hann window, 50% overlap) to calculate a PSD for each parcel and a cross spectral density (CSD) for each pairwise combination of parcels. We did this for each subject individually and (temporally) standardised (z-transformed) the parcel time courses because calculating the P/CSDs[3]. We obtained a (subjects, parcels, frequencies) array for the PSDs and (subjects, parcels, parcels, frequencies) array for the CSDs.

Canonical frequency bands. The P/CSD is a function of frequency. In time-averaged MEG analysis, it is common to reduce the frequency dimension by studying the activity in a particular frequency band. In the current work, we look at the following frequency bands: δ (1-4 Hz), θ (4-8 Hz), α (8-13 Hz), β (13-24 Hz), γ (30-45 Hz). We have chosen the frequency range 13-24 Hz for β due to an artefact in the coherence observed in the range 24-30 Hz that could not be removed with notch filters.

Power maps. Averaging a PSD over a frequency band, we get a *power density*, which we simply refer to as the *power* in the frequency band. We calculated the power at each parcel for each subject by averaging a PSD within the five canonical frequency bands described above. This resulted in a [subjects, parcels] array for each frequency band.

Each [parcels,1] array is referred to as a *power map*, which we can visualise as a heat map plot on the brain surface. Normally, when visualising a power map we're interested in looking at the power relative to a reference. In the time-averaged power analysis, we used the weighted (parcel-specific) average across frequency bands as the reference. This shows the spatial pattern of band-specific power relative to the power across all frequency bands. This was only done in the visualisation of group-averaged power maps.

Coherence networks/maps. We calculated the coherence using the P/CSD for each pairwise combination of parcels for each subject as

$$C_{xy} = \frac{|CSD_{xy}|}{\sqrt{PSD_x\, PSD_y}}, \tag{1}$$

where $|.|$ denotes the absolute value and x, y indicate different parcels. This resulted in a [subjects, parcels, parcels, frequencies] array. Averaging over the frequency dimension, we obtained a [subjects, parcels, parcels] array for each canonical frequency band.

Each [parcels, parcels] array represents a graphical network. The off-diagonal elements in the (parcels, parcels) array represent *edges* in the network. The graphical network was visualised by first subtracting a reference, which is the (edge-specific) weighted average across frequency bands, then thresholding to show the top 3% irrespective of sign. The colour of each edge indicates its value. The centroid of each parcel was used for the location of each node in the network.

We calculated a *coherence map* by averaging over the edges for each parcel, which resulted in a [parcels,1] array that can be visualised in the same way as a power map. We used the original [parcels, parcels] array before subtracting the reference and thresholding for this.

2.3 Transient Network Analysis

We used the method introduced in [9] to learn transient networks of coherent activity in source localised MEG data. This method applies a machine learning approach for segmenting time series data, known as the Hidden Markov Model (HMM, described below), on time-delay embedded (TDE)-PCA data. Figure S5 summarises the calculation of transient networks using this approach. We describe each step below.

[3]The PSD of standardised data is often referred to as the *relative PSD*.

2.3.1 Data Preparation

Before applying the HMM, the parcel time courses were prepared by performing TDE, which augments the data with extra channels containing time-lagged versions of the original data. In the current work, we used ±7 lags (±28 ms window), resulting in 780 channels. PCA was then applied at the group level to reduce the TDE data down to 120 channels. Finally, we (temporally) standardised (z-transformed) the TDE-PCA data. These were the data used to train the HMM.

2.3.2 The Hidden Markov Model

The HMM [44, 45] is a generative model for time series data. At each time point, t, there is an underlying categorical hidden state, $\theta_t \in \{1, ..., K\}$, where K is the number of states. The observed time series, $\boldsymbol{x}_t$, is generated using a multivariate Normal distribution based on the hidden state:

$$\boldsymbol{x}_t|(\theta_t = k) \sim \mathcal{N}(0, \boldsymbol{D}_k), \tag{2}$$

where $\theta_t = k$ is the state at time point t and $\boldsymbol{D}_k$ is a *state covariance*. Note, we force the mean to be zero to focus on modelling dynamics in the covariance, which contains the connectivity information we are interested in. Dynamics are governed by transitions in the hidden state. Note, it is assumed that the probability of a transition at time point t only depends on the state at the previous time point θ_{t-1} (this is the Markovian constraint). Each pairwise state transition probability is contained in the *transition probability matrix*:

$$A_{i,j} = p(\theta_t = j|\theta_{t-1} = i). \tag{3}$$

When we train an HMM on data, we learn the most likely value for the state covariances, $\{\boldsymbol{D}_1, ..., \boldsymbol{D}_K\}$, and transition probability matrix, $\boldsymbol{A}$, to have generated the data. We use stochastic variational Bayes [45] to do this, where we iteratively update our estimates for $\{\boldsymbol{D}_1, ..., \boldsymbol{D}_K, \boldsymbol{A}\}$ based on a random subset of the training data to minimise the variational free energy. We use the Baum-Welch algorithm [45] to calculate the (*posterior*) probability of each state being active at each time point, $q(\theta_t)$, for each subject based on our estimates for $\{\boldsymbol{D}_1, ..., \boldsymbol{D}_K, \boldsymbol{A}\}$. The posterior, $q(\theta_t)$, is a (states, time) array for each subject.

Hyperparameters. We used the HMM implemented in the `osl-dynamics` [61] toolbox. In order to train an HMM, we need to specify a few hyperparameters. An important hyperparameters is the number of states. In the current work, we identified 10 states for comparability with previous HMM MEG studies [9, 61, 46, 47, 48, 49, 50, 51, 52, 53, 54, 55], which used 6-12 states. Other hyperparameters include the batch size, sequence length and learning rates. These had little impact on the HMM inference. The values used are summarised in Table S1.

Run-to-run variability. The final estimates for $\{\boldsymbol{D}_1, ..., \boldsymbol{D}_K, \boldsymbol{A}\}$ can be sensitive to the initial values used at the start of training. The typical approach for overcoming this is to train several models from scratch starting from random initialisation and picking the one with the lowest final variational free energy (deemed the best description of the data) for the subsequence analysis. Historically, this has produced very reproducible results [61]. In our case, we analyse a particularly large dataset. This makes the HMM inference very stable, and we consistently converge on very similar estimates for $\{\boldsymbol{D}_1, ..., \boldsymbol{D}_K, \boldsymbol{A}\}$. Despite this, we took a cautionary approach and selected the best model from a set of five runs for analysis.

2.3.3 Post-Hoc Analysis

Once we trained an HMM and obtained a state probability time course for each subject, $q(\theta_t)$, we calculated a *state time course* by taking the most probable state (*maximum a posteriori probability estimate*) at each time point, $\hat{\theta}_t$. We then performed post-hoc analyses for each

subject using $\hat{\theta}_t$. Note, $\hat{\theta}_t$ is mutually exclusive, i.e. only one state is active at a given time point.

Summary statistics for dynamics. Each HMM state activation represents a transient network of coherent activity. Therefore, we can summarise the dynamics of each transient network by calculating summary statistics based on its state time course. For each subject and state, we calculated:

- Fractional occupancy: the fraction of total time spent in a state.
- Mean lifetime (ms): the average duration a state was active.
- Mean interval (s): the average duration between successive state activations.
- Switching rate (Hz): the average number of state activations per second.

These summary statistics are highly correlated. We will sometimes refer to them all jointly as the *occurrence*. An 'increased occurrence' refers to an increase in fractional occupancy, mean lifetime, switching rate and decrease in mean interval jointly.

Transition probabilities. We calculated a subject-specific transition probability matrix by counting the number of pairwise transitions for each combination of states in the state time course and normalising to ensure a sum-to-one constraint.

State power/coherence spectra. Here, we combined the state time course with the original parcel data (pre-TDE-PCA) to estimate the spectral properties (PSD and coherence) of each state using a multitaper [56]. This involved performing the following steps for each subject and state:

1. Temporally standardise the parcel time courses and multiply by the state time course.
2. Calculate P/CSD for each parcel/pair of parcels using a multitaper (2 s window, 0% overlap, 7 DPSS tapers, 4 Hz time half bandwidth). This is the standard approach/settings used for HMMs trained on TDE-PCA data [9, 54].
3. Use Equation (1) to calculate the coherence from the P/CSD.
4. The amplitude of the PSD is biased by the amount of time each state is active due to the multiplication in step 1. We account for this by scaling the PSD by one over the fractional occupancy of the state.

State power maps. The multitaper results in a [subjects, states, parcels, frequencies] array containing the PSDs. Similar to the time-averaged power analysis, we need to reduce the frequency dimension by averaging over a band. The HMM's objective is to identify spectrally distinct states, i.e. temporally segment occurrences of different oscillatory activity. Therefore, each HMM state tends to have its own characteristic PSD. This means we do not need to specify the frequency band by hand and can integrate over the full frequency range the of the PSD. Note, in practice we only calculated the PSD for the frequency range 1-80 Hz due to the bandpass filter we applied before source localisation. Averaging over the frequency dimension results in a [subjects, states, parcels] array. In the visualisation of the group-averaged power maps, we displayed each state's power map separately and used the average (parcel-specific) power across states as the reference.

State coherence networks/maps. The multitaper results in a [subjects, states, parcels, parcels, frequencies] array for the coherences. Similar to the state power maps, we reduce the frequency dimension by taking the average across the full frequency range (1-80 Hz). This results in a [subjects, states, parcels, parcels] array, which represent the state coherence networks. These are visualised in the same way as the time-averaged coherence networks. We displayed the group-average coherence network for each state individually using the (edge-specific) average across

states as the reference and thresholding the top 3% of edges irrespective of sign. The state coherence maps were calculated in the same way as the time-averaged coherence map using the non-referenced, unthresholded state coherence networks.

2.4 Statistical Significance Testing

In the current work, we characterised the impact of healthy ageing on resting-state functional networks by using a General Linear Model (GLM) with an age regressor to predict summary features calculated from the networks. The summary features used were: the power and coherence within canonical frequency bands from time-averaged networks (described in Section 2.2); and power, coherence and summary statistics for dynamics for the transient networks identified by the HMM (described in Section 2.3). We describe the procedures used for statistical significance testing below.

GLM permutations. We employed non-parametric permutations with a GLM [57] to test for statistical significance. This involved fitting a group-level model:

$$\boldsymbol{y} = \boldsymbol{X}\boldsymbol{\beta} + \boldsymbol{\epsilon}, \tag{4}$$

where $\boldsymbol{y}$ [subjects, features] is the target data, $\boldsymbol{X}$ [subjects, regressors] are regressors, referred to as the *design matrix*, $\boldsymbol{\beta}$ [regressors, features] are regression coefficients, referred to as *parameter estimates* or *effects*, and $\boldsymbol{\epsilon}$ [subjects, features] are the residuals.

For a given $\boldsymbol{X}$, fitting the group-level GLM to $\boldsymbol{y}$ provides an (ordinary-least-squares) estimate of $\boldsymbol{\beta}$ and $\boldsymbol{\epsilon}$. The effect $\boldsymbol{\beta}_i$ for regressor $\boldsymbol{X}_i$ indicates how $\boldsymbol{y}$ would change with $\boldsymbol{X}_i$. $\boldsymbol{\beta}_i$ is a [features,1] array and $\boldsymbol{X}_i$ is a [subjects,1] array.

Statistical significance testing involves defining a *COPE* (Contrast of Parameter Estimates) and building a *null distribution* of test statistics based on the COPE. We do this by repeatedly permuting the design matrix and refitting the GLM. We describe this in more detail below.

2.4.1 Age Effects

We are particularly interested in correlations with age, i.e. $\boldsymbol{\beta}_i$ for when $i = \text{Age}$. We refer to $\boldsymbol{\beta}_{\text{Age}}$ as the *age effect*.

Confounds. Isolating the change in functional brain activity due to age is difficult due to the many confounding variables that change with age and the heterogeneity in functional brain activity across subjects. Here, we include a comprehensive set of confounds: sex, total brain volume, relative grey matter volume, relative white matter volume, head size, (x, y, z) head position, and the PCA-reduced cognitive performance score. The grey/white volumes are relative to the total brain volume. The brain volumes were calculated from the sMRIs using FSL's anatomical processing script (`fsl_anat`). The head size and position were estimated by fitting a sphere to the Polhemus head shape points and fiducials. The design matrix used to study age effects is shown in Figure S6. We standardise each regressor (z-transform across the subject dimension) and include a constant (mean) regressor.

Statistical significance testing. We tested the following COPE for statistical significance,

$$|\boldsymbol{\beta}_{\text{Age}}| > 0, \tag{5}$$

where $|.|$ denotes the absolute value. Equation (5) tests whether $\boldsymbol{\beta}_{\text{Age}}$ is significantly different from zero. We built a null distribution for $\boldsymbol{\beta}_{\text{Age}}$ by randomly permuting the design matrix $\boldsymbol{X}$, refitting the GLM, and recording the maximum COPE across all features (i.e. $\max(|\boldsymbol{\beta}_{\text{Age}}|)$) as the *test statistic*.

By taking the maximum COPE, we account for multiple comparisons. We used the COPE as the test statistic rather than a (one sample) t-statistic because the variance of each feature was very different. This violated the exchangeability assumption (that the distribution for

each feature is the same) implicit in the maximum statistic approach for multiple comparison correction [57]. The high variance in particular features reduces the t-statistic and sensitivity to effects in the features. In all permutation testing we used the maximum COPE as the test statistic apart from when looking at linear age effects in the summary statistics for dynamics, where we used the maximum t-statistic due to the different scale of each features[4]. In the transient network analysis, we took the maximum COPE across all networks.

We applied 1,000 random 'sign-flip' permutations to the age regressor, where each entry in $\boldsymbol{X}_{\text{Age}}$ had a 50% chance of being multiplied by -1. This resulted in a null distribution of size 1000. Looking up the percentile at which the observed COPE (calculated with the non-permuted design matrix) occurs in the null distribution gave us our p-value. We got a p-value for each feature. Sufficiently small p-values (< 0.05) were deemed to be significant.

2.4.2 Cognitive Performance Effects

We were also interested in functional brain activity that correlates with cognitive performance. This is given by $\boldsymbol{\beta}_{\text{Cog. Perf.}}$, which is referred to as the *cognitive performance effect*.

Confounds. The PCA-reduced cognitive score (see Section 2.1) is negatively correlated with age (see Figure S2). We need to be sure that any effect we observed from the cognitive score is not simply indirectly due to the age effect. In order to do this, we included age as a confound regressor in the design matrix used to study the cognitive performance effect, see Figure S6. We also included same the brain volume and head size/position confounds we did when we studied the linear age effect. Including the age regressor in the design matrix can be seen as a conservative approach as this is the equivalent of regressing out the age effect from the target data (and other regressors).

Statistical significance testing. We tested the following COPE for statistical significance,

$$|\boldsymbol{\beta}_{\text{Cog. Perf.}}| > 0. \tag{6}$$

We used the same procedure for building the null distribution (1,000 sign-flip permutations) and calculating a p-value as we did for the linear age effect. We used the maximum COPE as the test statistic in all cases apart from when predicting the summary statistics for dynamics, where we used the maximum t-statistic instead. We took the maximum COPE across all transient networks to correct for multiple comparisons.

[4]Fractional occupancy, mean lifetime, mean interval and switching rate.

3 Results

Healthy individuals exhibit frequency-specific networks of oscillatory activity

Figure 1 shows the power spectral density (PSD), coherence spectrum and time-averaged networks for a large cohort of healthy individuals ($N = 612$, 18-88 years old).

The PSD decreases with frequency and there is a prominent peak in the α band, which indicates there are strong α oscillations present in the data (Figure 1A, left). Note, the dataset contained eyes closed resting-state MEG recordings, which are known to contain strong α activity [3]. The PSD is characterised with FOOOF [60] in SI 1.1. The coherence spectrum is approximately flat except for the peak in the α band, which reflects phase locking between the α oscillations (Figure 1A, right). There is an artefact in the PSD and coherence spectrum between 24 and 30 Hz, which could not be removed with notch filters, therefore, this frequency range was not included in our definition of the β-band.

Figure 1B shows the spatial distribution of power in five canonical frequency bands (δ, θ, α, β, γ) and Figure 1C shows the coherence maps. The visualisation of the power and coherence maps highlights the activity unique to each band (the weighted mean across frequency bands was used as the reference). Low frequencies (δ, θ) have relatively high frontal power/coherence and low posterior coherence. The α band has relatively high occipital power and coherence. The β band has relatively high sensorimotor power and low posterior coherence. The γ band has globally low power but high posterior coherence particularly in the temporal regions.

Unique spectral changes are observed with age in the time-averaged networks for each canonical frequency band

Figure 2 shows age effects in time-averaged networks for each canonical frequency band.

The power and coherence in time-averaged networks follow a unique trajectory for each canonical frequency band (Figure 2A). Power in the δ and θ band decreases with age and coherence increases. Power in the α and γ remains stable with age but coherence decreases. Power and coherence in the β band increase with age.

Turning to the region-specific age effects in power (Figure 2B), there is: a decrease in global-δ power; increase in temporal-α power; increase in occipital-θ power, which reflects a slowing (leftward shift) of the α peak (Figure S3); and an increase in sensorimotor and frontal-β activity. Turning to the region-specific coherence age effects (Figure 2C), there is a general increase for all frequencies apart from the α band.

Time-averaged posterior α-band activity increases with cognitive performance

Figure 3 shows cognitive performance effects in time-averaged networks. By accounting for age as a confound (see Section 2.4.2), we isolated the correlation with power and coherence that cannot be explained by age (nor any other confound, such as brain volume or head size/position).

Whilst accounting for age, good cognitive performance correlates with increased posterior-α power (Figure 3A) and coherence (Figure 3B). That is, the cognitive performance effects oppose age effects in the α band (Figure 2).

Healthy individuals exhibit fast ($\sim$ 100 ms) transient networks of coherent activity

Figure 4 shows ten transient networks identified in a large cohort of healthy individuals ($N = 612$, 18-88 years old).

Each network corresponds to a unique transient pattern of power and coherence. The visualisation of the power maps and coherence networks in Figure 4A highlights the differences in each transient network from the time-averaged activity. E.g. when State 1 is active there is increased global power and parietal/temporal/frontal coherence; when State 2 is active there is

increased sensorimotor power and coherence, etc. These transient networks have been found in multiple previous studies [9, 61]. However, this study has identified these networks in the largest cohort to date.

The transient networks have fast dynamics with average lifetimes of less than 100 ms (Figure 4D). The probability of transitions between networks shows some structure (Figure 4C). For example, State 1 has a higher probability of transitioning to another positively activated state (States 2-4). There is also a relatively high probability of remaining in State 1 and 10 once activated, which is reflected in the higher mean lifetime for these states (Figures 4C and D).

Frontal transient networks increase in global connectivity and decrease in occurrence

Figure 5 shows age effects in the spectral properties and dynamics of transient networks.

The frontal networks (States 4 and 9) are particularly affected by age. Both show an increase in global coherence (Figure 5B). The other higher-order networks (States 1 and 10) show a decrease in global coherence (Figure 5B).

There are two groups of states that show opposing age effects in dynamics. Most states (1, 2, 5, 6, 7, 8 and 10) show an increase in stay probability, which results in an increased occurrence with age. In contrast, States 4 and 9 show a decrease in stay probability, which results in a decreased occurrence with age.

Frontal transient network dynamics are related to cognitive performance

Figure 6 shows the cognitive performance effects for transient networks and their dynamics.

Increased coherence in the frontal network (State 4) correlates with good cognitive performance (Figure 6B) as well as reduced switching into this network (Figure 6D).

An increase in the stay probability of State 2 and State 8 was also observed (Figure 6C). These networks represent activity in the primary visual and sensorimotor regions respectively. The increased stay probability of these networks underpins the increase in posterior-α activity and sensorimotor-β activity that was observed in the cognitive performance effects in time-averaged networks (Figure 3).

4 Discussion

4.1 Previous Neuroimaging Findings

For reviews of M/EEG ageing studies, see [12, 13, 14]. For a review of MRI ageing studies, see [66].

4.1.1 Resting-State M/EEG

Time-averaged networks. Several studies have reported age effects in time-averaged oscillatory power. A decrease in low-frequency power (δ, θ) and increase in high-frequency power (β, γ) have consistently been reported [15, 16, 17, 18, 19, 20]. However, there is significant heterogeneity across studies in the regions affected. The findings in the current work support the observation that low-frequency power decreases and high-frequency power increases with age (Figure 2B).

Age effects in α-band power are less clear with both increases and decreases previously being reported in MEG studies [15, 16, 18, 21]. This is due to the spatial heterogeneity in α-band power changes. In the current work, a decrease in occipital-α power due to the slowing (leftward shift) of the α-peak frequency (Figure S3B) and increase in temporal-α power (Figure 2B) was observed. These findings are consistently reported in the EEG literature [62, 63, 64, 65] and have recently been observed in MEG [21].

Turning to age effects in time-averaged functional connectivity, Stier and colleagues [15] found a global increase in θ and γ connectivity and a global decrease in α connectivity with age (using imaginary coherence as the measure of connectivity). In the current work, the same findings have been observed albeit with a different measure for connectivity (coherence, Figure 2C).

Transient networks. Only two studies have looked at transient functional networks inferred using MEG data: [25, 26]. Both used a HMM to infer the transient networks. Several of the transient networks presented in [25] are found here despite some differences in how the data were prepared for the HMM. Here, we used time-delay embedding to model dynamics in the cross spectral properties (coherence) of the data [61], whereas [25] focused on the dynamics of amplitude covariances.

Most of the age effects of the transient networks reported in [25] were also found here. However, two transient networks in [25] show opposite age effects in occurrence relative to our work. First, Tibon's frontal network (FTP2) increases in occurrence, whereas our corresponding frontal network (State 4) decreases. Second, Tibon's visual network (EV2) decreases in occurrence, whereas our corresponding visual network (State 8) increases. Both discrepancies arise due to differences in modelling the transient networks. In the current work, each transient network is modelled as a unique spatiospectral (i.e. amplitude and frequency) pattern of activity, whereas in Tibon's work each transient network is modelled as a spatial (amplitude only) pattern of activity. The transient networks we identify underpin the frequency-specific age effects observed in the time-averaged power (Figure 2B). The decrease in time-averaged δ power with age is underpinned by a decrease in the frontal network (State 4) occurrence (Figure 5D). The decrease in time-averaged occipital-α power with age is underpinned by a reduction of within network power of State 8 (Figure 5A) in combination with the increased occurrence (Figure 5D). In other words, although the visual network (State 8) has a higher occurrence, the occipital-α power when it activates is decreased with age.

Tibon and colleagues [25] also linked the occurrence of transient networks to cognitive performance. They found better cognitive performers (in terms of fluid intelligence) had lower occurrences of frontoparietotemporal networks and higher occurrences of visual networks whilst accounting for age. Our findings support this with an increased occurrence of the visual network (State 8) and decreased occurrence of the frontal network (State 4) despite using a different

metric for cognitive performance[5] (Figure 6D).

Overall, apart from the direction of age effects in dynamics for the frontal (State 4) and visual network (State 8), the two studies agree reasonably well in terms of the changes to dynamics with age and their link to cognition.

Coquelet and colleagues [26] have reported several results (in the Elderly − Adult group contrast) that are reproduced here. They reported an increase in time-averaged global-β power, which we find as a sensorimotor/frontal power increase in the β band (Figure 2B). They used the same approach as Tibon and colleagues [25] to model dynamics in amplitude covariances to identify transient networks with an HMM. They reported an increased occurrence for the left and right auditory networks with age, which we also find (States 5 and 6, Figure 5D). They also reported a decrease in occurrence of the visual network with age (similar to the finding in [25]), which is the opposite age effect in the dynamics of our visual network (State 8). This discrepancy is for the same reason as with Tibon's work (modelling dynamics in oscillatory properties vs amplitude). Overall, apart from the age effect of the visual network (State 8), our findings agree reasonably well with those of Coquelet and colleagues.

4.1.2 Resting-State fMRI (Networks)

A well-established finding in the fMRI literature is the existence of functional networks in resting-state activity [70, 71]. The same functional networks are recruited in cognitive tasks [72, 73] suggesting that the underlying functional architecture that underpins cognition can be studied via the resting-state networks. For a review of ageing studies in fMRI resting-state networks, see [74, 75, 76, 77].

Comparing directly between the MEG and fMRI networks is difficult for a number of reasons, including: the difference in the underlying signal being measured (postsynaptic currents in MEG, BOLD for fMRI [78]); differences in the measure for functional connectivity (coherence for MEG, correlation in fMRI); and differences in the network modelling (the HMM assumes only one state is activate at a given time point, whereas the spatial ICA used in fMRI allows temporally overlapping networks [70, 71]). Nevertheless, we summarise the key findings from resting-state fMRI below and comment on the perspective provided by MEG.

Within and between network functional connectivity. The fMRI literature reports there is a decrease in the within-network functional connectivity with age for most resting-state fMRI networks and an increase in the functional connectivity between networks [74]. In the MEG description, we observe heterogeneous changes across the networks (Figure 5B). Whereas within-network connectivity decreases with age in States 1, 2, 3, and 10, and increases in States 4 and 9. Due to the mutual exclusivity assumption of the HMM, we do not assess inter-network connectivity in MEG.

In particular, the fMRI default mode network has consistently been reported to decrease in functional connectivity with age [74, 75, 76, 77]. In the current work, State 1 (Figure 4) most closely resembles the fMRI default mode network [7, 55] given of the overlap in regions showing high activity in MEG and fMRI (frontal and parietal). In the MEG default mode network, we observe a global decrease in functional connectivity with age (coherence, Figure 5B), supporting the fMRI finding.

Network dynamics. A reduction in resting-state fMRI network dynamics, i.e. a reduced ability to switch between network states, with age has consistently been reported [74]. In the current work, we find the rate of switching into two frontal networks (States 4 and 9, Figure 5D) are especially reduced with age, supporting the fMRI finding. Cabral and colleagues [79] related the switching rate of resting-state fMRI networks to cognitive performance (a PCA-reduced battery of cognitive test scores). Comparing older adults with good and poor cognitive performance, they found reduced switching rates and longer state lifetimes correlated with better

[5] We used the PCA-reduced cognitive score, see Section 2.1.

performance. Our findings support this, despite the difference in the time scale of switching[6]. In particular, we find that a reduction in the rate of switching into the frontal network (State 4, Figure 6D) correlates with good cognitive performance.

4.1.3 Task fMRI

There are two main observations for age-related changes from task fMRI studies that have consistently been reported. These are discussed below.

PASA. This is a decrease in posterior activity and increase in anterior activity observed during task performance for older participants compared to younger participants [69]. Although, the current work has looked at resting-state MEG, our results do support this observation with decreasing time-averaged δ power in posterior regions and increasing β power in anterior regions with age (Figure 2B). The age effects in connectivity (Figure 2C), however, suggest most regions increase in connectivity with age and we do not observe any clear spatial gradient for connectivity changes.

Turning to the transient network analysis, we see that the majority of states show a PASA trend in oscillatory power (Figure 5A). This raises the speculative possibility that PASA may affect all transient functional networks for example through a change to the underlying physiology of the brain.

Hemispheric Asymmetry Reduction in Old Adults (HAROLD). This is the observation that older participants show less lateralised activity in frontal regions compared to younger participants in memory tasks [67]. In the current work, we found little evidence in support of HAROLD. This may be because we are studying resting-state MEG data, although HAROLD has been reported in resting-state fMRI [68].

HAROLD suggests we should expect less lateralised activity with increasing age. A result of note in the current work is the observation that the left temporal network (State 5) shows a larger increase in fractional occupancy and mean lifetime (underpinned by the increased stay probability) with age compared to the right temporal network (State 6), see Figure 5D. The significantly increased power in the left temporal network (State 5, Figure 5A) further supports greater age effects in the left temporal lobe compared to the right. This suggests resting-state functional activity in MEG may in fact be more lateralised with age, at least in the temporal lobes, which is an observation that directly opposes HAROLD.

4.2 Cognitive Ageing Theories

Cognitive decline is considered a normal consequence of ageing. Yet, there is broad variability with some individuals managing to preserve their cognitive abilities with age [80]. Here, we studied a large cohort of individuals that show some cognitive decline across multiple domains with age (Figure S2). These individuals were deemed to be healthy by the Cam-CAN study [27, 28]. A question that arises is what aspects of brain function supports healthy cognitive ageing. We consider two potentially co-occurring mechanisms hypothesised to mediate cognitive health in ageing: *maintenance* and *compensation* [81]. For a review of cognitive ageing theories in relation to observations from neuroimaging, see [82, 83].

Maintenance. This is the idea that individuals preserve their cognitive abilities by maintaining the integrity of relevant neural resources (structural and functional), see Figure 7C. A prediction of this theory is that the cognitive performance effect should be in the opposite direction to age effects, i.e. those that have good cognitive performance (whilst accounting for age) have biologically younger looking brains in terms of their functional activity. Indeed, in the time-averaged analyses, we found posterior-α activity was positively correlated with cognitive performance (Figure 3) but negatively correlated with age (Figure 2). This supports the

[6] fMRI network dynamics are on time scales of seconds, where MEG network dynamics are on time scales of ~ 100 milliseconds.

maintenance hypothesis. Note, we have observed this in a cross-sectional study. To determine conclusively whether the maintenance of α activity negates cognitive decline, a longitudinal study is required.

Compensation. This is the idea that individuals preserve their cognitive ability despite a failure to maintain the integrity of relevant neural resources (e.g. structural) by engaging some compensatory functional activity. For example, individuals might have white matter integrity that is degrading with age and a functional network that has increased activity with age, see Figure 7B. A prediction of this theory is that the cognitive performance effect should be in the same direction as age effects, i.e. those that have good cognitive performance (whilst accounting for age) appear to have biologically older looking brains in terms of their functional activity. Indeed, we found the properties of a frontal transient network (State 4) correlated with cognitive performance and age in the same way (Figures 6 and 5 respectively) suggesting changes to this network are compensatory. Once again, we should be clear that we have observed this in a cross-sectional study.

Speculatively, the age and cognitive performance effects of the frontal networks could be interpreted as an increase in efficiency: less frequent, shorter visits are observed suggesting less time is needed for the frontal network to performance cognition. The reverse maybe true for the remaining networks, i.e. a reduction in efficiency indicated by more frequent, longer visits.

Another interesting speculative hypothesis is that the time-averaged and transient networks reflect two different aspects of the organisation of functional brain activity. The time-averaged activity could reflect the underlying *scaffolding* [84] of functional activity, i.e. the time-invariant patterns of functional activity that the brain can support. The maintenance of this scaffolding enables an individual to preserve their cognitive abilities. The transient networks could reflect the dynamic coordination of functional activity based upon the scaffolding. Here, an individual utilises compensation to preserve their cognitive abilities.

4.3 Clinical Disease Studies

In the clinical study of diseases, such as Alzheimer's or Parkinson's disease, age is an important confound. To understand pathological changes in the brain due to disease, we must first characterise age-related changes in the healthy brain, especially the changes expected due to healthy ageing. The current work goes towards this aim by characterising the large-scale functional networks found in a large cohort of healthy individuals. We have made these functional networks (time-averaged and transient) publicly available, see Section 6. These can be used as a point of comparison in clinical MEG studies. Example scripts for inferring dynamics on new M/EEG data based on a basis set of healthy networks are also provided. This can be a potentially useful resource for researchers studying diseases with MEG.

5 Conclusions

Tables 2 and 3 summarise (statistically significant) age effects in time-averaged and transient functional networks respectively. Clearly, there are many age effects in the functional brain networks of healthy individuals.

Multiple age effects were observed in the time-averaged power and coherence. Different changes occur for different regions and frequencies. The changes in time-averaged power are consistent with the PASA observation in fMRI. Relating the time-averaged networks to cognitive health, we found evidence for the maintenance of functional activity preserving healthy cognitive ageing: less biological ageing in posterior-α activity was implicated in better cognitive performance.

We then used a transient network description to provide a more detailed view of functional brain activity that is inaccessible to time-averaged approaches. We identified ten transient networks with unique spatiospectral properties and fast dynamics. Multiple age effects were observed across all networks, both in the power and coherence within a network and in their dynamics. We observed age effects in the dynamics of transient networks, whereby the frontal networks (States 4 and 9) decreased in occurrence with age, whilst all of other networks increased. The frontal network was also implicated in cognitive health. The correlations of this network with age and cognitive performance suggested that the changes were compensatory.

In sum, our findings show many age effects should be expected for time-averaged and transient functional brain networks for healthy individuals. We show the dynamics of the transient networks are correlated with age and are related to cognitive performance. Our results show that both maintenance and compensation mechanisms can contribute to preserved cognitive health with ageing. We provide the functional networks calculated in the current work as a public resource to characterise a healthy brain, which may be useful for understanding when an individual deviates from a healthy trajectory due to disease.

Table 2: Age effects in in time-averaged functional networks. ↑ denotes an increase with age and ↓ denotes a decrease.

Frequency Band	**Power**	**Coherence**
δ (1-4 Hz)	Global ↓	Global ↑
θ (4-8 Hz)	Sensorimotor/frontal ↓	-
α (8-13 Hz)	Temporal ↑	Sensorimotor/temporal ↓
β (13-24 Hz)	Sensorimotor ↑	Frontal ↑
γ (30-45 Hz)	-	Temporal ↑

Table 3: Age effects in in transient functional networks. ↑ denotes an increase with age and ↓ denotes a decrease. Symbols/acronyms: probability of transitioning from state i to j ($A_{i,j}$); probability of remaining in state i ($A_{i,i}$); fractional occupancy (FO); mean lifetime (LT); mean interval (INTV); switching rate (SR).

State	**Power**	**Coherence**	**Dynamics**
1	Temporal ↑	Parietal/sensorimotor ↓	$A_{1,1}$ ↑
2	Sensorimotor ↑	Sensorimotor ↓	$A_{2,2}$ ↑, FO ↑, LT ↑
3	Occipital ↓	Occipital ↓	-
4	Prefrontal ↑	Global ↑	$A_{1-7,4}$ ↓, FO ↓, LT ↓, INTV ↑ , SR ↓
5	Left temporal ↑	-	$A_{4-5,5}$ ↑, FO ↑, LT ↑
6	-	-	$A_{6,6}$ ↑, FO ↑, LT ↑
7	-	-	$A_{7,7}$ ↑, FO ↑, LT ↑
8	-	-	$A_{8-9,8}$ ↑, FO ↑, INTV ↓
9	-	Global ↑	$A_{7-10,9}$ ↓, FO ↓, LT ↓, INTV ↑, SR ↓
10	-	Global ↓	$A_{9,10}$ ↑

6 Data Availability and Code

Access to the Cam-CAN dataset can be requested here [29]. Python scripts for reproducing the analysis in the current work starting from the public data are available here: `https://github.com/OHBA-analysis/Gohil2024_AgeEffectsRSNs`. The time-averaged and transient networks calculated in the current work are also provided.

7 Funding

This research was supported by the National Institute for Health Research (NIHR) Oxford Health Biomedical Research Centre. The Wellcome Centre for Integrative Neuroimaging is supported by core funding from the Wellcome Trust (203139/Z/16/Z). CG is supported by the Wellcome Trust (215573/Z/19/Z). OK is supported by the Marie Sklodowska-Curie Innovative Training Network "European School of Network Neuroscience (euSNN)" (860563). MWJvE is supported by the Wellcome Trust (106183/Z/14/Z, 215573/Z/19/Z), the New Therapeutics in Alzheimer's Diseases (NTAD) supported by the MRC and the Dementia Platform UK (RG94383/RG89702). DV is supported by a Novo Nordisk Foundation Emerging Investigator Fellowship (NNF19OC-0054895), an ERC Starting Grant (ERC-StG-2019-850404), and a DFF Project 1 from the Independent Research Fund of Denmark (2034-00054B). MRT is supported by the Motor Neurone Disease Association. ACN is supported by the Wellcome Trust (104571/Z/14/Z) and James S. McDonnell Foundation (220020448). MWW is supported by the Wellcome Trust (106183/Z/14/Z, 215573/Z/19/Z), the New Therapeutics in Alzheimer's Diseases (NTAD) study supported by UK MRC, the Dementia Platform UK (RG94383/RG89702) and the NIHR Oxford Health Biomedical Research Centre (NIHR203316). The views expressed are those of the author(s) and not necessarily those of the NIHR or the Department of Health and Social Care.

8 Competing Interests

No competing interests.

References

[1] World Health Organization. (2021). Decade of healthy ageing: baseline report. World Health Organization.

[2] Fred, A. L., Kumar, S. N., Kumar Haridhas, A., Ghosh, S., Purushothaman Bhuvana, H., Sim, W. K. J., ... & Gulyás, B. (2022). A brief introduction to magnetoencephalography (MEG) and its clinical applications. Brain sciences, 12(6), 788.

[3] Buzsáki, G. (2006). *Rhythms of the Brain*. Oxford university press.

[4] Bressler, S. L., & Menon, V. (2010). Large-scale brain networks in cognition: emerging methods and principles. Trends in cognitive sciences, 14(6), 277-290.

[5] Voytek, B., & Knight, R. T. (2015). Dynamic network communication as a unifying neural basis for cognition, development, aging, and disease. Biological psychiatry, 77(12), 1089-1097.

[6] Fries, P. (2015). Rhythms for cognition: communication through coherence. Neuron, 88(1), 220-235.

[7] Brookes, M. J., Woolrich, M., Luckhoo, H., Price, D., Hale, J. R., Stephenson, M. C., ... & Morris, P. G. (2011). Investigating the electrophysiological basis of resting state networks using magnetoencephalography. Proceedings of the National Academy of Sciences, 108(40), 16783-16788.

[8] Proudfoot, M., Woolrich, M. W., Nobre, A. C., & Turner, M. R. (2014). Magnetoencephalography. Practical neurology, 14(5), 336-343.

[9] Vidaurre, D., Hunt, L. T., Quinn, A. J., Hunt, B. A., Brookes, M. J., Nobre, A. C., & Woolrich, M. W. (2018). Spontaneous cortical activity transiently organises into frequency specific phase-coupling networks. Nature communications, 9(1), 2987.

[10] Hillebrand, A., & Barnes, G. R. (2005). Beamformer analysis of MEG data. International review of neurobiology, 68, 149-171.

[11] Matthews, P. M., & Jezzard, P. (2004). Functional magnetic resonance imaging. Journal of Neurology, Neurosurgery & Psychiatry, 75(1), 6-12.

[12] Jauny, G., Eustache, F., & Hinault, T. T. (2022). M/EEG dynamics underlying reserve, resilience, and maintenance in aging: a review. Frontiers in Psychology, 13, 861973.

[13] Maestú, F., Solesio-Jofre, E., & Bajo, R. (2019). Towards the Understanding of Healthy and Pathological Aging Through MEG. Magnetoencephalography: From Signals to Dynamic Cortical Networks, 817-851.

[14] Ishii, R., Canuet, L., Aoki, Y., Hata, M., Iwase, M., Ikeda, S., ... & Ikeda, M. (2018). Healthy and pathological brain aging: from the perspective of oscillations, functional connectivity, and signal complexity. Neuropsychobiology, 75(4), 151-161.

[15] Stier, C., Braun, C., & Focke, N. K. (2023). Adult lifespan trajectories of neuromagnetic signals and interrelations with cortical thickness. NeuroImage, 278, 120275.

[16] Rempe, M. P., Ott, L. R., Picci, G., Penhale, S. H., Christopher-Hayes, N. J., Lew, B. J., ... & Wilson, T. W. (2023). Spontaneous cortical dynamics from the first years to the golden years. Proceedings of the National Academy of Sciences, 120(4), e2212776120.

[17] Hoshi, H., & Shigihara, Y. (2020). Age-and gender-specific characteristics of the resting-state brain activity: a magnetoencephalography study. Aging (Albany NY), 12(21), 21613.

[18] Hunt, B. A., Wong, S. M., Vandewouw, M. M., Brookes, M. J., Dunkley, B. T., & Taylor, M. J. (2019). Spatial and spectral trajectories in typical neurodevelopment from childhood to middle age. Network Neuroscience, 3(2), 497-520.

[19] Marek, S., Tervo-Clemmens, B., Klein, N., Foran, W., Ghuman, A. S., & Luna, B. (2018). Adolescent development of cortical oscillations: Power, phase, and support of cognitive maturation. PLoS biology, 16(11), e2004188.

[20] Gómez, C., Pérez-Macías, J. M., Poza, J., Fernández, A., & Hornero, R. (2013). Spectral changes in spontaneous MEG activity across the lifespan. Journal of neural engineering, 10(6), 066006.

[21] Quinn, A. (2024). Big MEG GLM paper. In preparation.

[22] Schlee, W., Leirer, V., Kolassa, I. T., Weisz, N., & Elbert, T. (2012). Age-related changes in neural functional connectivity and its behavioral relevance. BMC neuroscience, 13, 1-11.

[23] Schlee, W., Leirer, V., Kolassa, S., Thurm, F., Elbert, T., & Kolassa, I. T. (2012). Development of large-scale functional networks over the lifespan. Neurobiology of aging, 33(10), 2411-2421.

[24] Jauny, G., Eustache, F., & Hinault, T. (2022). Connectivity dynamics and cognitive variability during aging. Neurobiology of Aging, 118, 99-105.

[25] Tibon, R., Tsvetanov, K. A., Price, D., Nesbitt, D., Cam, C. A., & Henson, R. (2021). Transient neural network dynamics in cognitive ageing. Neurobiology of aging, 105, 217-228.

[26] Coquelet, N., Wens, V., Mary, A., Niesen, M., Puttaert, D., Ranzini, M., ... & De Tiège, X. (2020). Changes in electrophysiological static and dynamic human brain functional architecture from childhood to late adulthood. Scientific Reports, 10(1), 18986.

[27] Shafto, M. A., Tyler, L. K., Dixon, M., Taylor, J. R., Rowe, J. B., Cusack, R., ... & Cam-CAN. (2014). The Cambridge Centre for Ageing and Neuroscience (Cam-CAN) study protocol: a cross-sectional, lifespan, multidisciplinary examination of healthy cognitive ageing. BMC neurology, 14, 1-25.

[28] Taylor, J. R., Williams, N., Cusack, R., Auer, T., Shafto, M. A., Dixon, M., ... & Henson, R. N. (2017). The Cambridge Centre for Ageing and Neuroscience (Cam-CAN) data repository: Structural and functional MRI, MEG, and cognitive data from a cross-sectional adult lifespan sample. neuroimage, 144, 262-269.

[29] `https://camcan-archive.mrc-cbu.cam.ac.uk/dataaccess/`.

[30] Borgeest, G. S., Henson, R., Shafto, M., Samu, D., & Kievit, R. (2018). Greater lifestyle engagement is associated with better cognitive resilience.

[31] Quinn, A. J., van Es, M., Gohil, C., & Woolrich, M. W. (2022). Ohba software library in python (osl). Zenodo https://doi. org/10.5281/ZENODO, 6875060.

[32] Taulu, S., Simola, J., & Kajola, M. (2005). Applications of the signal space separation method. IEEE transactions on signal processing, 53(9), 3359-3372.

[33] Rosner, B. (1983). Percentage points for a generalized ESD many-outlier procedure. Technometrics, 25(2), 165-172.

[34] Hyvarinen, A. (1999). Fast and robust fixed-point algorithms for independent component analysis. IEEE transactions on Neural Networks, 10(3), 626-634.

[35] Perrin, F., Pernier, J., Bertrand, O., & Echallier, J. F. (1989). Spherical splines for scalp potential and current density mapping. Electroencephalography and clinical neurophysiology, 72(2), 184-187.

[36] Smith, S. M. (2002). Fast robust automated brain extraction. Human brain mapping, 17(3), 143-155.

[37] Jenkinson, M. (2005). BET2: MR-based estimation of brain, skull and scalp surfaces. In Eleventh Annual Meeting of the Organization for Human Brain Mapping, 2005.

[38] Henson, R. N., Mattout, J., Phillips, C., & Friston, K. J. (2009). Selecting forward models for MEG source-reconstruction using model-evidence. Neuroimage, 46(1), 168-176.

[39] Van Veen, B. D., & Buckley, K. M. (1988). Beamforming: A versatile approach to spatial filtering. IEEE assp magazine, 5(2), 4-24.

[40] Tait, L., Özkan, A., Szul, M. J., & Zhang, J. (2021). A systematic evaluation of source reconstruction of resting MEG of the human brain with a new high-resolution atlas: Performance, precision, and parcellation. Human Brain Mapping, 42(14), 4685-4707.

[41] Kohl, O., Woolrich, M., Nobre, A. C., & Quinn, A. (2023). Glasser52: A parcellation for MEG-Analysis [Data set]. Zenodo. https://doi.org/10.5281/zenodo.10401793.

[42] Colclough, G. L., Brookes, M. J., Smith, S. M., & Woolrich, M. W. (2015). A symmetric multivariate leakage correction for MEG connectomes. Neuroimage, 117, 439-448.

[43] Welch, P. (1967). The use of fast Fourier transform for the estimation of power spectra: A method based on time averaging over short, modified periodograms. IEEE Transactions on audio and electroacoustics, 15(2), 70-73.

[44] Rabiner, L., & Juang, B. (1986). An introduction to hidden Markov models. ieee assp magazine, 3(1), 4-16.

[45] Bishop, C. M. (2006). Pattern recognition and machine learning. Springer google schola, 2, 1122-1128.

[46] Quinn, A. J., Vidaurre, D., Abeysuriya, R., Becker, R., Nobre, A. C., & Woolrich, M. W. (2018). Task-evoked dynamic network analysis through hidden Markov modeling. Frontiers in neuroscience, 12, 603.

[47] Higgins, C., Liu, Y., Vidaurre, D., Kurth-Nelson, Z., Dolan, R., Behrens, T., & Woolrich, M. (2021). Replay bursts in humans coincide with activation of the default mode and parietal α networks. Neuron, 109(5), 882-893.

[48] Gohil, C., Roberts, E., Timms, R., Skates, A., Higgins, C., Quinn, A., ... & Woolrich, M. (2022). Mixtures of large-scale dynamic functional brain network modes. NeuroImage, 263, 119595.

[49] van Es, M. W., Higgins, C., Gohil, C., Quinn, A. J., Vidaurre, D., & Woolrich, M. W. (2023). Large-scale cortical networks are organized in structured cycles. bioRxiv, 2023-07.

[50] Kohl, O., Gohil, C., Zokaei, N., Hu, M. T., Nobre, A. C., Woolrich, M., & Quinn, A. (2024). Changes in sensorimotor network dynamics in resting-state recordings in Parkinson's Disease. medRxiv, 2024-01.

[51] Gohil, C., Kohl, O., Huang, R., van Es, M. W., Jones, O. P., Hunt, L. T., ... & Woolrich, M. W. (2024). Dynamic Network Analysis of Electrophysiological Task Data. bioRxiv, 2024-01.

[52] Cho, S., van Es, M. W., Woolrich, M. W., & Gohil, C. (2024). Comparison between EEG and MEG of static and dynamic resting-state networks. bioRxiv, 2024-04.

[53] Vidaurre, D., Abeysuriya, R., Becker, R., Quinn, A. J., Alfaro-Almagro, F., Smith, S. M., & Woolrich, M. W. (2018). Discovering dynamic brain networks from big data in rest and task. NeuroImage, 180, 646-656.

[54] Vidaurre, D., Quinn, A. J., Baker, A. P., Dupret, D., Tejero-Cantero, A., & Woolrich, M. W. (2016). Spectrally resolved fast transient brain states in electrophysiological data. Neuroimage, 126, 81-95.

[55] Baker, A. P., Brookes, M. J., Rezek, I. A., Smith, S. M., Behrens, T., Probert Smith, P. J., & Woolrich, M. (2014). Fast transient networks in spontaneous human brain activity. elife, 3, e01867.

[56] Babadi, B., & Brown, E. N. (2014). A review of multitaper spectral analysis. IEEE Transactions on Biomedical Engineering, 61(5), 1555-1564.

[57] Winkler, A. M., Ridgway, G. R., Webster, M. A., Smith, S. M., & Nichols, T. E. (2014). Permutation inference for the general linear model. Neuroimage, 92, 381-397.

[58] Gramfort, A., Luessi, M., Larson, E., Engemann, D. A., Strohmeier, D., Brodbeck, C., ... & Hämäläinen, M. (2013). MEG and EEG data analysis with MNE-Python. Frontiers in neuroscience, 7, 70133.

[59] Maris, E., & Oostenveld, R. (2007). Nonparametric statistical testing of EEG-and MEG-data. Journal of neuroscience methods, 164(1), 177-190.

[60] Donoghue, T., Haller, M., Peterson, E. J., Varma, P., Sebastian, P., Gao, R., ... & Voytek, B. (2020). Parameterizing neural power spectra into periodic and aperiodic components. Nature neuroscience, 23(12), 1655-1665.

[61] Gohil, C., Huang, R., Roberts, E., van Es, M. W., Quinn, A. J., Vidaurre, D., & Woolrich, M. W. (2024). osl-dynamics, a toolbox for modeling fast dynamic brain activity. Elife, 12, RP91949.

[62] Tröndle, M., Popov, T., Pedroni, A., Pfeiffer, C., Barańczuk-Turska, Z., & Langer, N. (2023). Decomposing age effects in EEG α power. Cortex, 161, 116-144.

[63] Scally, B., Burke, M. R., Bunce, D., & Delvenne, J. F. (2018). Resting-state EEG power and connectivity are associated with α peak frequency slowing in healthy aging. Neurobiology of aging, 71, 149-155.

[64] Klass, D. W., & Brenner, R. P. (1995). Electroencephalography of the elderly. Journal of Clinical Neurophysiology, 12(2), 116-131.

[65] Babiloni, C., Binetti, G., Cassarino, A., Dal Forno, G., Del Percio, C., Ferreri, F., ... & Rossini, P. M. (2006). Sources of cortical rhythms in adults during physiological aging: a multicentric EEG study. Human brain mapping, 27(2), 162-172.

[66] Dennis, N. A., & Cabeza, R. (2011). Neuroimaging of healthy cognitive aging. In The handbook of aging and cognition (pp. 1-54). Psychology Press.

[67] Cabeza, R., Anderson, N. D., Locantore, J. K., & McIntosh, A. R. (2002). Aging gracefully: compensatory brain activity in high-performing older adults. Neuroimage, 17(3), 1394-1402.

[68] Li, Z., Moore, A. B., Tyner, C., & Hu, X. (2009). Asymmetric connectivity reduction and its relationship to "HAROLD" in aging brain. Brain research, 1295, 149-158.

[69] Davis, S. W., Dennis, N. A., Daselaar, S. M., Fleck, M. S., & Cabeza, R. (2008). Que PASA? The posterior–anterior shift in aging. Cerebral cortex, 18(5), 1201-1209.

[70] Beckmann, C. F., DeLuca, M., Devlin, J. T., & Smith, S. M. (2005). Investigations into resting-state connectivity using independent component analysis. Philosophical Transactions of the Royal Society B: Biological Sciences, 360(1457), 1001-1013

[71] Calhoun, V. D., Kiehl, K. A., & Pearlson, G. D. (2008). Modulation of temporally coherent brain networks estimated using ICA at rest and during cognitive tasks. Human brain mapping, 29(7), 828-838.

[72] Cole, M. W., Bassett, D. S., Power, J. D., Braver, T. S., & Petersen, S. E. (2014). Intrinsic and task-evoked network architectures of the human brain. Neuron, 83(1), 238-251.

[73] Cole, M. W., Ito, T., Bassett, D. S., & Schultz, D. H. (2016). Activity flow over resting-state networks shapes cognitive task activations. Nature neuroscience, 19(12), 1718-1726.

[74] Deery, H. A., Di Paolo, R., Moran, C., Egan, G. F., & Jamadar, S. D. (2023). The older adult brain is less modular, more integrated, and less efficient at rest: A systematic review of large-scale resting-state functional brain networks in aging. Psychophysiology, 60(1), e14159.

[75] Damoiseaux, J. S. (2017). Effects of aging on functional and structural brain connectivity. Neuroimage, 160, 32-40.

[76] Sala-Llonch, R., Bartrés-Faz, D., & Junqué, C. (2015). Reorganization of brain networks in aging: a review of functional connectivity studies. Frontiers in psychology, 6, 136321.

[77] Ferreira, L. K., & Busatto, G. F. (2013). Resting-state functional connectivity in normal brain aging. Neuroscience & Biobehavioral Reviews, 37(3), 384-400.

[78] de Beeck, H. O., & Nakatani, C. (2019). Introduction to human neuroimaging. Cambridge University Press.

[79] Cabral, J., Vidaurre, D., Marques, P., Magalhães, R., Silva Moreira, P., Miguel Soares, J., ... & Kringelbach, M. L. (2017). Cognitive performance in healthy older adults relates to spontaneous switching between states of functional connectivity during rest. Scientific reports, 7(1), 5135.

[80] Glisky, E. L. (2007). Changes in cognitive function in human aging. Brain aging, 3-20.

[81] Cabeza, R., Albert, M., Belleville, S., Craik, F. I., Duarte, A., Grady, C. L., ... & Rajah, M. N. (2018). Maintenance, reserve and compensation: the cognitive neuroscience of healthy ageing. Nature Reviews Neuroscience, 19(11), 701-710.

[82] McDonough, I. M., Nolin, S. A., & Visscher, K. M. (2022). 25 years of neurocognitive aging theories: What have we learned?. Frontiers in Aging Neuroscience, 14, 1002096.

[83] Grady, C. (2012). The cognitive neuroscience of ageing. Nature Reviews Neuroscience, 13(7), 491-505.

[84] Reuter-Lorenz, P. A., & Park, D. C. (2014). How does it STAC up? Revisiting the scaffolding theory of aging and cognition. Neuropsychology review, 24, 355-370.

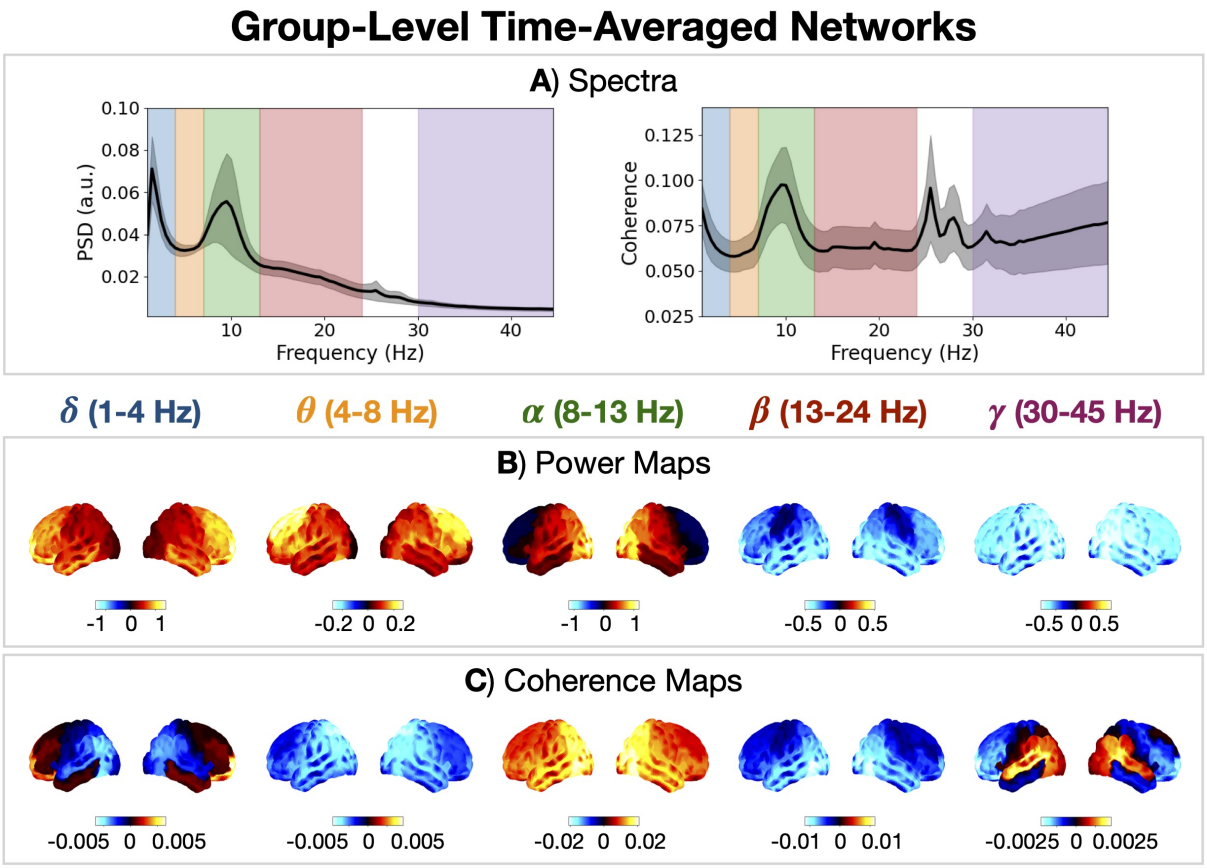

Figure 1: **Healthy individuals exhibit frequency-specific networks of oscillatory activity**. PSD (A, left) and coherence spectrum (A, right) averaged over parcels and subjects. The grey shaded area shows the standard deviation across subjects. Power (B) and coherence (C) maps for each canonical frequency band relative to the weighted mean across frequency bands.

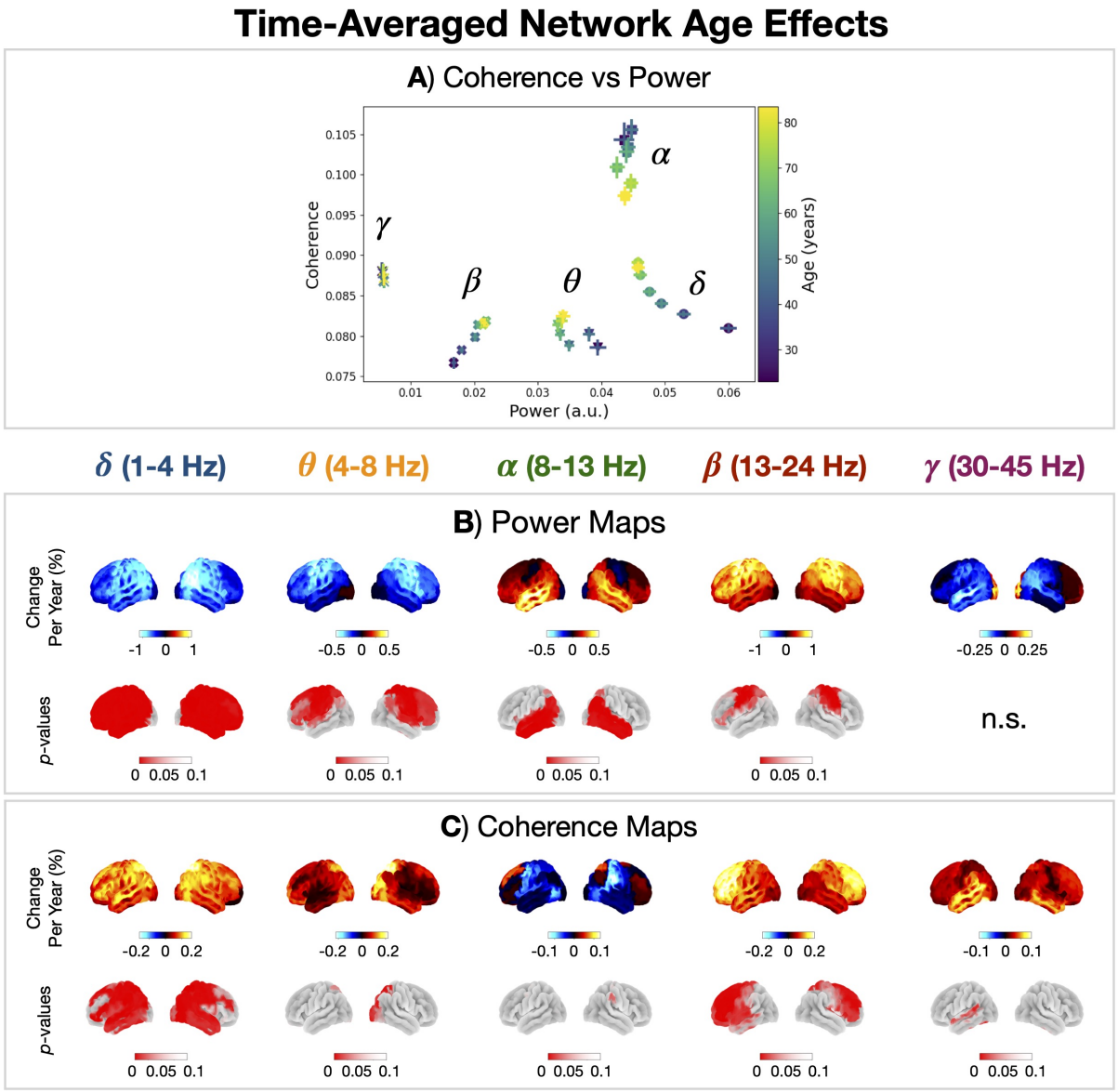

Figure 2: **Unique spectral changes are observed with age in the time-averaged networks for each canonical frequency band**. A) Coherence vs power for each canonical frequency band averaged over frequencies, parcels and subjects for different 10 year cohorts (18-28, 28-38, ..., 78-88 years old). The error bar shows the standard error on the mean. Age effects in power (B) and coherence (C) for each canonical frequency band.

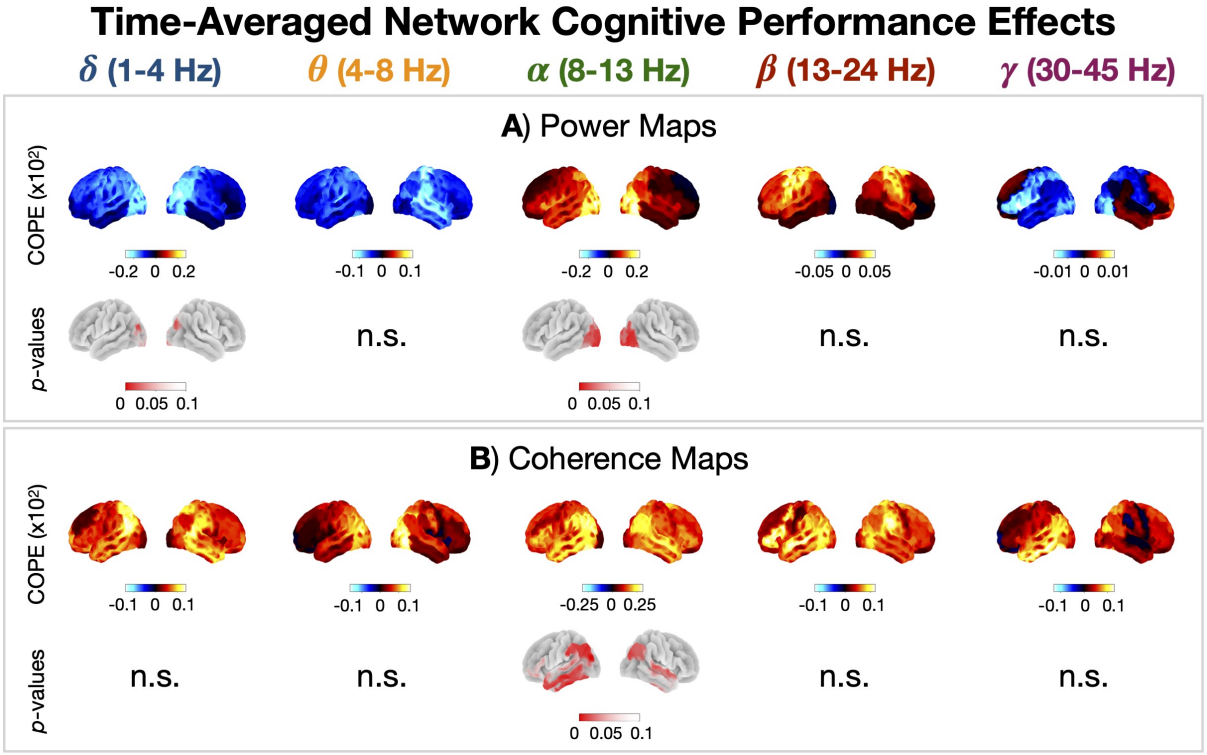

Figure 3: **Time-averaged posterior alpha-band activity increases with cognitive performance**. Cognitive performance effects in power (A) and coherence (B) for each canonical frequency band.

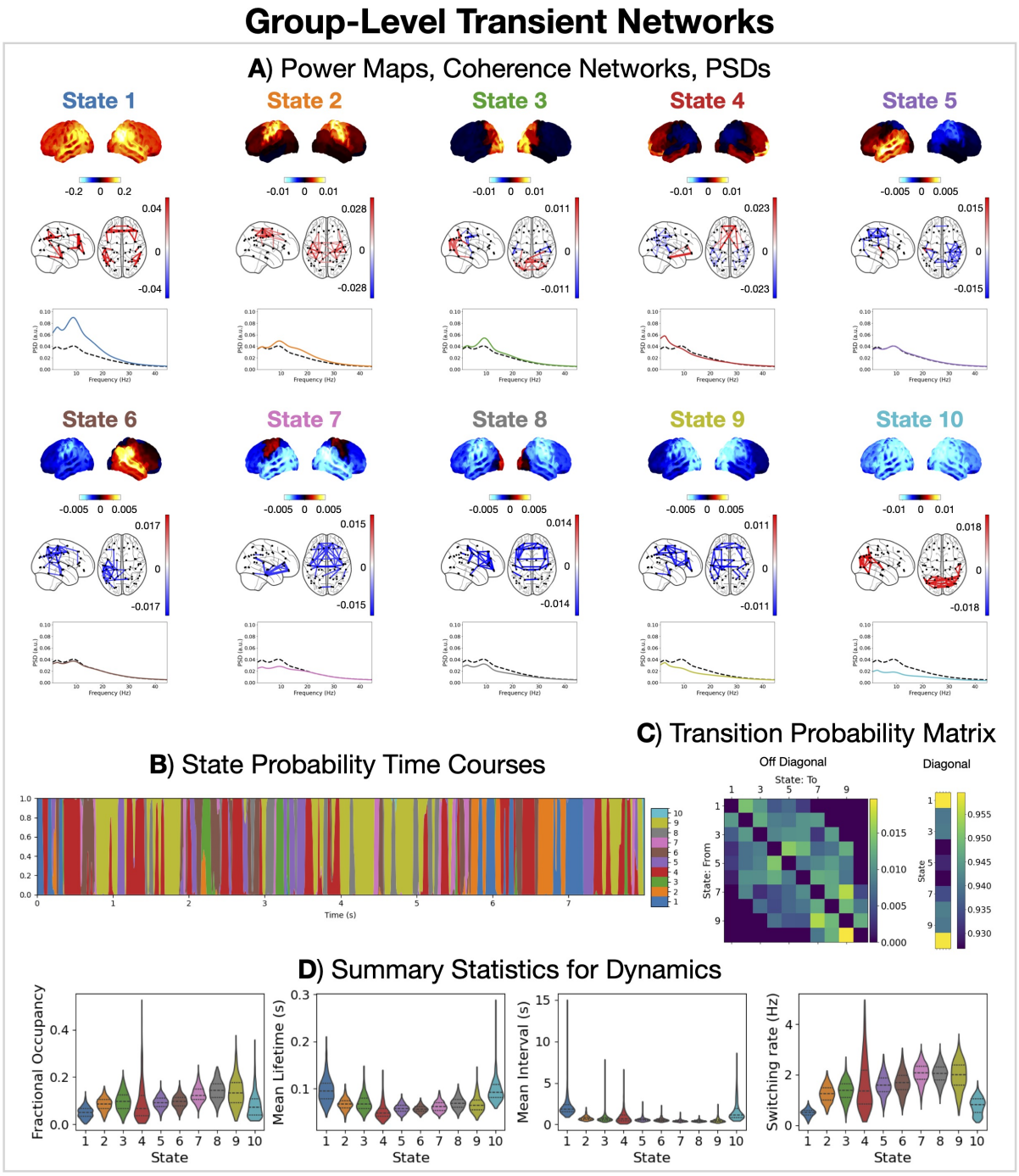

Figure 4: **Healthy individuals exhibit fast (∼100 ms) transient networks of coherent activity**. A) Power maps and coherence networks (top 3% of edges) averaged over subjects for each state and PSD averaged over subjects and parcels for each state. Power maps and coherence networks are shown relative to the average across states. The black dashed line in the state PSDs shows the time-averaged PSD. B) Inferred state probability time courses. Note, only the first 8 seconds for the first subject has been shown for illustration. C) Inferred state transition probability matrix. D) Distribution of summary statistics for dynamics across subjects. The states are ordered in terms of decreasing total power.

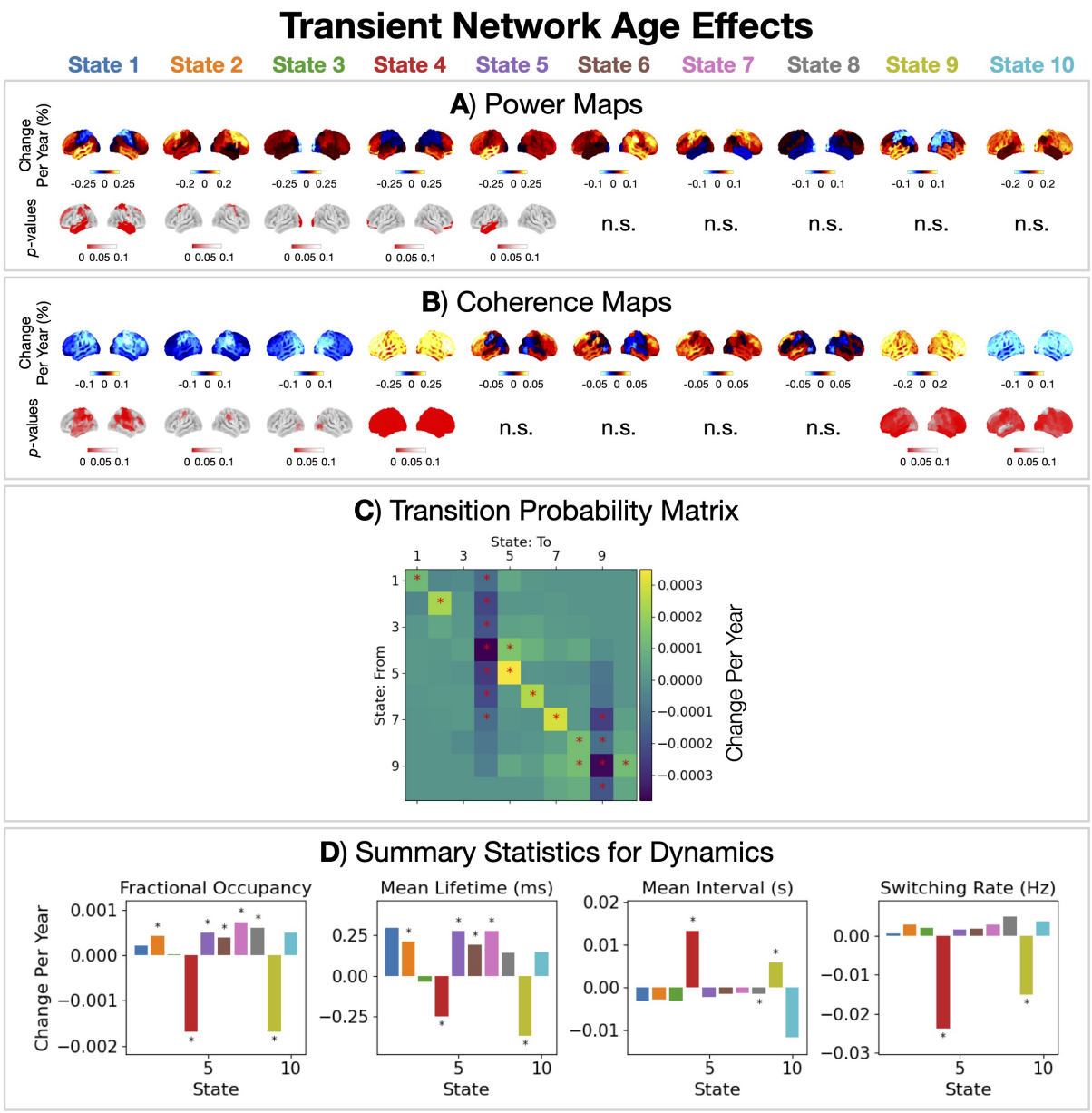

Figure 5: **Frontal transient networks increase in global connectivity and decrease in occurrence**. Age effects in power (A), coherence (B), transition probabilities (C) and summary statistics for dynamics (D) for each HMM state. The asterisks indicate a p-value < 0.05.

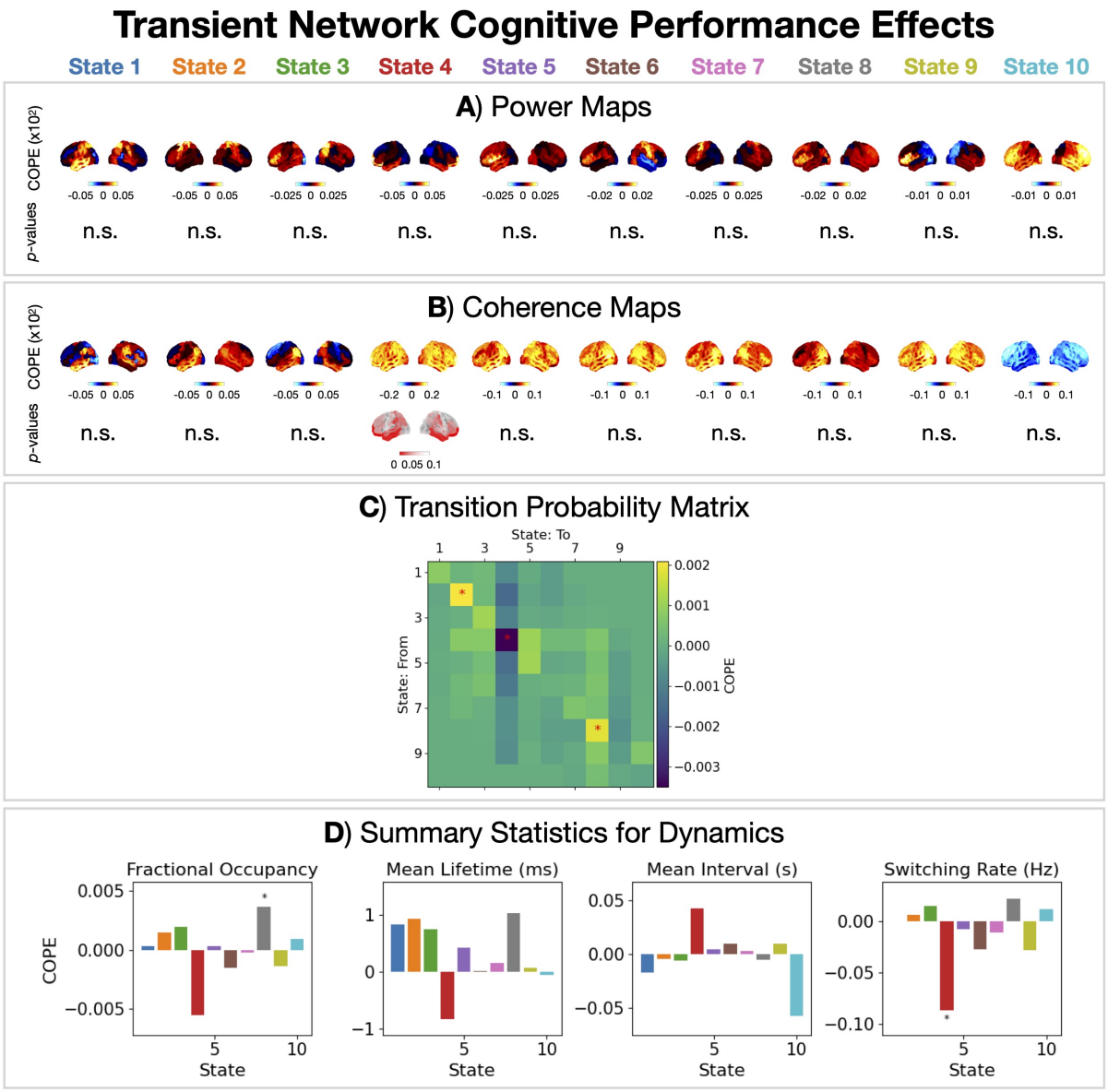

Figure 6: **Frontal transient network dynamics are related to cognitive performance**. Cognitive performance effects in power (A), coherence (B), transition probabilities (C) and summary statistics for dynamics (D) for each HMM state. The asterisks indicate a p-value < 0.05.

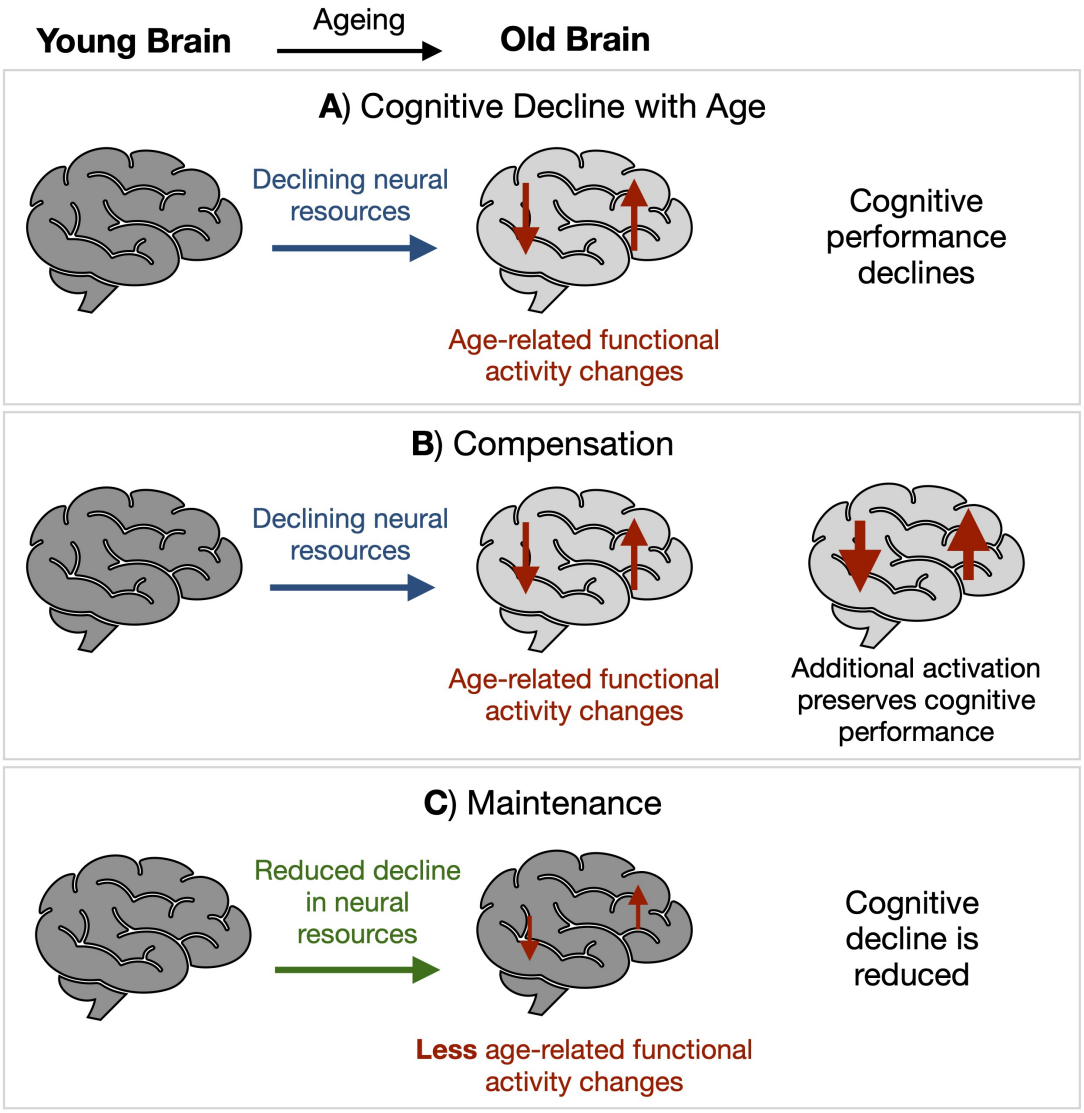

Figure 7: **Mechanisms for preserving cognitive health with age**. A) Changes in functional activity that occur with age. B) The compensation hypothesis. C) The maintenance hypothesis.